Hydration of a calcium sulfoaluminate cement blended with zincite

Gwenn Le Saoût
Professor, LMGC, IMT Mines Ales, Univ Montpellier, CNRS, Ales, France
(corresponding author: gwenn.le-saout@mines-ales.fr)
(Orcid:0000-0002-2761-0584)

Dominique Lafon-Pham
Professor, EuroMov Digital Health in Motion, IMT Mines Ales,
Univ Montpellier, Ales, France

Jean Claude Roux
Research Engineer, Centre des Matériaux de l'École des mines d'Alès
(C2MA), IMT Mines Alès, University of Montpellier, Alès, France

A calcium sulfoaluminate (CSA) cement has been characterised by X-ray diffraction and energy-dispersive X-ray spectroscopy analysis. Selective extraction methods have been used to improve detection limits for identification and quantitative measurements. Perovskites are present in the cement in the form of brownmillerite and a phase with the following average chemical composition $Ca_{1.95}Mg_{0.05}Al_{0.29}Ti_{0.39}Fe_{1.03}Si_{0.22}O_{5.18}$. The zincite is known as a strong retarder for ordinary Portland cement (OPC), and its effect on the hydration of CSA cement was investigated using isothermal calorimetry, thermal analysis and X-ray diffraction. The low pH of the pore solution in the CSA cement compared to the OPC considerably reduces the solubility of zincite and, at an early age of hydration, zincite behaves as a filler in the CSA cement.

Keywords: microstructure/modelling/
special cements

Introduction

The first patent for a calcium sulfoaluminate (CSA) cement was taken out in 1935 (Établissements Poliet & Chausson, 1935). CSA cements were mainly used as expansive binders in the 1950s (Klein and Troxell, 1958) before their development for structural applications by the China Building Material Academy in the 1970s (Zhang *et al.*, 1999). CSA cements have many specific properties compared to Portland cements, such as fast setting, rapid hardening and shrinkage reduction. This special cement used alone or in combination with calcium sulfates and Portland cement has found applications such as airport runways and road patching, self-levelling mortars, tile adhesive grouts and so on (Zhang *et al.*, 1999). This is also a promising alternative to Portland cement with a low carbon dioxide (CO_2) footprint, owing to the difference in energy used to produce CSA cements (lower kiln temperatures and energy at the mill to grind) and the lower mass of carbon dioxide emitted during the clinkering reaction (Gartner, 2004). The main raw materials used for making CSA cements are bauxite, limestone, clay and gypsum, and this leads to a wide range of mineralogical composition different from that of Portland cements (Wang and Su, 1994). CSA cements may be classified according to the content of ye'elimite (Aranda and De la Torre, 2013; Odler, 2000)

- calcium sulfoaluminate clinkers which contain ye'elimite or kleinite, Klein's salt or tetracalcium trialuminate sulfate ($C_4A_3\bar{S}$) with a content varying between 50 and 90 mass%
- belite CSA clinkers containing belite (C_2S) (40–50 mass%) as the main phase and a lower amount of ye'elimite (20–30 mass%)
- alite CSA clinkers containing alite and ye'elimite.

In this study, a commercial CSA cement was used. CSA clinkers were usually co-grinded with 15 to 25 mass% of calcium sulfate to optimise strength development and volume changes (Winnefeld and Barlag, 2009). The first part of this study was dedicated to the characterisation of the anhydrous CSA cement as only few studies are available concerning the characterisation of CSA cements (García-Maté *et al.*, 2015).

Zinc oxide (ZnO) can get into Portland cement in different ways. It may be introduced from zinc present in the clinker (Bolio-Arceo and Glasser, 1998), from industrial waste stabilised using cementitious materials (Fernández Olmo *et al.*, 2001) or from galvanised steel reinforcements (Belaïd *et al.*, 2001). It can be used as a rebar corrosion inhibitor (De Rincón *et al.*, 2002), for its photocatalytic properties or for the purpose of self-cleaning materials (Senff *et al.*, 2014). However, zincite is particularly known as a strong hydration retarder for Portland cement (Arliguie and Grandet, 1985; Ataie *et al.*, 2015) and alkali-activated slag (Garg and White, 2017) and this can restrict the possible applications of zincite. The mechanism of retardation in these systems is still controversial. The formation of a zinc hydroxide ($Zn(OH)_2$) phase on the cement particle surfaces preventing further dissolution, as first proposed by Arliguie and Grandet (1985), was not experimentally observed and the retardation was subsequently explained by the depletion of calcium in solution by the formation of a calcium zincate phase (Garg and White, 2017) or by nucleation and growth poisoning of calcium silicate hydrate (C–S–H) (Ataie *et al.*, 2015). Although many studies have been carried out on the effect of zinc oxide on the hydration of Portland cements, the aim of the present study is to investigate the effect of zincite on early-age hydration of a commercial CSA cement.

Materials and methods

Materials

The chemical composition of the CSA cement is given in Table 1. Zincite (ZnO extra S, ZnO > 99·9 mass%, $d_{50} = 6$ μm) was from Silar. Quartz from Sifraco ($d_{50} = 11$ μm) was used as a chemically inert material for the calorimetric experiments. In order to check the effect of particle size, the quartz was also milled to $d_{50} = 7$ μm in a McCrone micronising mill. Mixtures of the CSA cement with 10 mass% of the zincite or quartz were prepared by co-grinding the materials by hand in an agate mortar for 15 min.

Table 1. Mineralogical and chemical compositions of the CSA cement

Oxides	Mass %	Phases	Mass %
Sodium oxide (Na_2O)	0·02	Yee'limite	31·4
Magnesium oxide (MgO)	1·27	Belite	21·2
Aluminium oxide (Al_2O_3)	19·1	Anhydrite	18·3
Silicon dioxide (SiO_2)	8·42	Gypsum	2·9
Phosphorus pentoxide (P_2O_5)	0·08	Perovskite	11·3
Sulfur trioxide (SO_3)	15·2	Ferrite	5·4
Potassium oxide (K_2O)	0·08	Calcite	3·5
Calcium oxide (CaO)	44·9	Dolomite	0·7
Titanium dioxide (TiO_2)	0·76	Periclase	0·6
Manganese oxide (MnO)	0·04	Merwinite	1·9
Iron (III) oxide (Fe_2O_3)	6·94	Magnesite	1·5
LOI[a]	3·3	Magnesioferrite	0·8
d_{10}: μm[b]	2	Magnetite	0·2
d_{50}: μm	7	Quartz	0·2
d_{90}: μm	19		
Density: g/cm^3	2·99		

Chemical analysis by XRF
[a]Loss on ignition (LOI) measured up to 950°C by TGA
[b]Particle size determined by laser granulometry

The pastes were formulated to have a water-to-cement ratio of 0·70. Samples consisting of 50 g of binder and the appropriate amount of water were mixed twice for 90 s with a high-shear blender (except for internal mixing in conduction calorimetry experiments).

Methods

The particle size distribution was measured by laser diffraction spectrometer LS 13 320 Beckman Coulter using the wet method with isopropyl alcohol for cement and deionised water for quartz and zincite as a dispersion medium. Ultrasonic treatment was used to improve the cement dispersion.

In order to analyse the mineralogical composition, X-ray diffraction (XRD) was performed with a diffractometer, the Bruker D8 Advance. Powder samples were analysed using an incident beam angle (Cu Kα, $\lambda = 0{\cdot}154$ nm) varying between 5 and 75°. X'Pert High Score Plus software (version 2.1) was used to process diffraction patterns and Rietveld analysis. The Inorganic Crystal Structure Database (ICSD) codes used for the Rietveld refinement are given in Table 2. For the in situ XRD analysis, the paste was cast into a sample holder positioned in a temperature-controlled stage from Mesicon at 25°C and covered by a Kapton polyimide film to prevent evaporation. An external standard zinc oxide (G-factor approach) was used to quantify the X-ray amorphous and crystalline non-quantified parts according to the method presented by Jansen *et al.* (2011) and applied to an ordinary Portland system. The mass attenuation coefficients of the samples were calculated using data from X-ray fluorescence analysis (Table 1).

For thermogravimetric analysis (TGA), plastic bottles of volume 12 ml were completely filled with the fresh paste; the

Table 2. References of the different phases used for Rietveld analysis

Phase	Formula	Crystal system	ICSD	Reference
Ye'elimite	$C_4A_3\bar{S}$	Orthorhombic	80361	Calos *et al.* (1995)
		Cubic	9560	Saalfeld and Depmeier (1972)
Belite	C_2S-β	Monoclinic	81096	Mumme *et al.* (1995)
	C_2S-α'_H	Orthorhombic	81097	Mumme *et al.* (1995)
Anhydrite	$C\bar{S}$	Orthorhombic	16382	Kirfel and Will (1990)
Gypsum	$C\bar{S}H_2$	Monoclinic	151692	De la Torre *et al.* (2004)
Perovskite	CT	Cubic	31865	Sasaki *et al.* (1987)
Ferrite	C_4AF	Orthorhombic	98827	Redhammer *et al.* (2004)
Calcite	$C\bar{C}$	Hexagonal	79674	Wartchow (1989)
Dolomite	$CM\bar{C}_2$	Hexagonal	31335	Effenberger *et al.* (1983)
Periclase	M	Cubic	104844	Taylor (1984)
Merwinite	C_3MS_2	Monoclinic	26002	Moore and Araki (1972)
Magnesite	$M\bar{C}$	Hexagonal	63663	Göttlicher and Vegas (1988)
Magnesioferrite	MF	Cubic	24229	Barth and Posnjak (1932)
Magnetite	Fe_3O_4	Cubic	29129	Sasaki (1997)
Quartz	S	Hexagonal	90145	Gualtieri (2000)
Ettringite	$C_6A\bar{S}_3H_{32}$	Hexagonal	155395	Goetz-Neunhoeffer and Neubauer (2006)
Gibbsite	AH_3	Monoclinic	27698	Saafeld and Wedde (1974)

bottles were sealed and stored at 25°C. Hydration was stopped by immersing small pieces (around 2–3 mm^3) for 30 min in isopropanol and rinsing twice with diethyl ether. TGA (Netzsch STA 449F5) was performed using about 50 mg of powder at a heating rate of 20°C/min under nitrogen between 30 and 950°C.

A conduction calorimeter (Tam Air, Thermometric AB, Sweden) operating at 25°C was used to determine the hydration heat flow. About 5 g of paste were weighed into sealed glass flasks and transferred into the calorimeter within 3 min. In order to study the very early hydration reactions (before 1 h), admix ampoules described by Wadsö (2005) were also used to enable internal mixing.

For the microscopic investigations of anhydrous samples, powder was impregnated using a low-viscosity epoxy resin and polished down to 0·25 μm using diamond pastes. The polished sections obtained were further coated with carbon (∼5 nm) and examined using a Quanta 200 FEG scanning electron microscope (SEM) from FEI coupled to an Oxford Xmax N 80 mm^2 energy-dispersive X-ray spectroscopy (EDX) analyser. The EDX analyses were used to determine the elemental compositions of the phase assemblage. The analyses were carried out using an acceleration voltage of 15 kV to ensure a good compromise between spatial resolution and adequate excitation of the FeK_α peak.

In order to improve the characterisation of the anhydrous cement, two different selective dissolution methods were used. In the first method, an aqueous solution of potassium hydroxide and sucrose was used to produce a residue rich in belite (Lejbina, 1969). In the second one, the silicate phases were removed in a solution of salicylic acid in methanol (SAM) (Hjorth and Lauren, 1971). In addition, ye'elimite, anhydrite and gypsum phases were dissolved in a 5% sodium carbonate (Na_2CO_3) solution (Wang, 2010) to obtain a residue with a high amount of perovskites. This method was modified to prevent precipitation of calcium carbonate ($CaCO_3$) by washing the filtered suspension with 6% acetic acid (AA) solution. The filter paper and contents were placed in an oven at 105°C until a constant weight was reached.

Thermodynamic modelling was carried out using the Gibbs free energy minimisation software GEMS v3.4 (Kulik *et al.*, 2013) with the thermodynamic database from PSI-GEMS (Hummel *et al.*, 2002) and the Cemdata 18·1 database specific to cement (Lothenbach *et al.*, 2019). Modelling was conducted in a similar manner as described before for the hydration of CSA cements (Le Saoût *et al.*, 2013; Winnefeld and Lothenbach, 2010). By combining experimental data based on the XRD-Rietveld analysis, which describes the dissolution of the cement phases as a function of time, with a thermodynamic equilibrium model, which assumes equilibrium between the solution and the hydrates, the amount and nature of hydrates formed can be described as a function of time.

The pH of the interstitial solution at early age was determined with a pH meter combined with an electrode, the Jenway Ion Meter 3345. The interstitial solution was obtained after mixing cement paste for 7 min, then the paste was centrifuged for 10 min at 10 000 r/min and filtered using 0·45 mm filter syringe.

Results and discussion

Characterisation of the CSA cement

The main phases observed in the experimental diffraction pattern (Figure 1) are the orthorhombic ye'elimite $C_4A_3\bar{S}$ with a small amount of the pseudo cubic form, belite β and α'_H- C_2S and perovskites from the CSA clinker. Anhydrite II $C\bar{S}$ is also present as a mineral addition. The molar ratio of gypsum and anhydrite to ye'elimite leads to a value of about 2·9 that corresponds to a self-stressing cement (Winnefeld and Barlag, 2010). The amount of belite obtained by Rietveld refinement (21 mass%) is close to the value calculated from the SAM extraction method (23 +/−2 mass%). The SAM–sodium carbonate–AA extraction method leads to an amount of perovskite, ferrite, magnesite, magnesioferrite, dolomite, quartz and periclase of around 15 mass%, in good agreement with the Rietveld analysis (15 mass%). The magnetite does not dissolve but is extracted by the bar magnet and it can be considered that the dissolution rate of dolomite in the presence of acetic acid is quite low compared to calcite and aragonite (Toyama and Terakado, 2015). According to the present result, the method seems quantitative but should be repeated with a large range of CSA cements. The perovskite family has crystal structures related to the mineral perovskite CT. Ferrite phase $Ca_2(Al_xFe_{1-x})_2O_5$ is usually present in CSA clinker and its structure is derived from that of perovskite by the substitution of Al and Fe for Ti, together with ordered omission of oxygen atoms, which causes one-half of the octahedral sheets in perovskite to be replaced by tetrahedral chains (Taylor, 1997). To improve Rietveld refinement, it is necessary to add a perovskite phase CT (Álvarez-Pinazo *et al.*, 2012). The titanium dioxide is present in the bauxite used as a raw material in the manufacturing process of CSA clinker. The peaks associated with this cubic phase are confirmed in the XRD pattern of the CSA after the extraction of the main phases (Figure 1(c)). EDX analysis on a polished section of the CSA (Figure 2) was used to determine the chemical composition of each phase of the anhydrous cement (Table 3). The CSA cement after extraction revealed an average composition of ferrite $Ca_{1·99}Al_{0·39}Si_{0·10}Fe_{1·35}Ti_{0·08}Mg_{0·07}O_{5·00}$ not far from the composition of the brownmillerite series $Ca_2(Fe_{2-x}Al_x)O_5$. However, the average composition of perovskite $Ca_{1·95}Mg_{0·05}Al_{0·29}Ti_{0·39}Fe_{1·03}Si_{0·22}O_{5·18}$ is far from the perovskite $Ca_2Ti_2O_4$ composition with, in some grains, perovskite lamellae with a high amount of Ti on the scale of a few

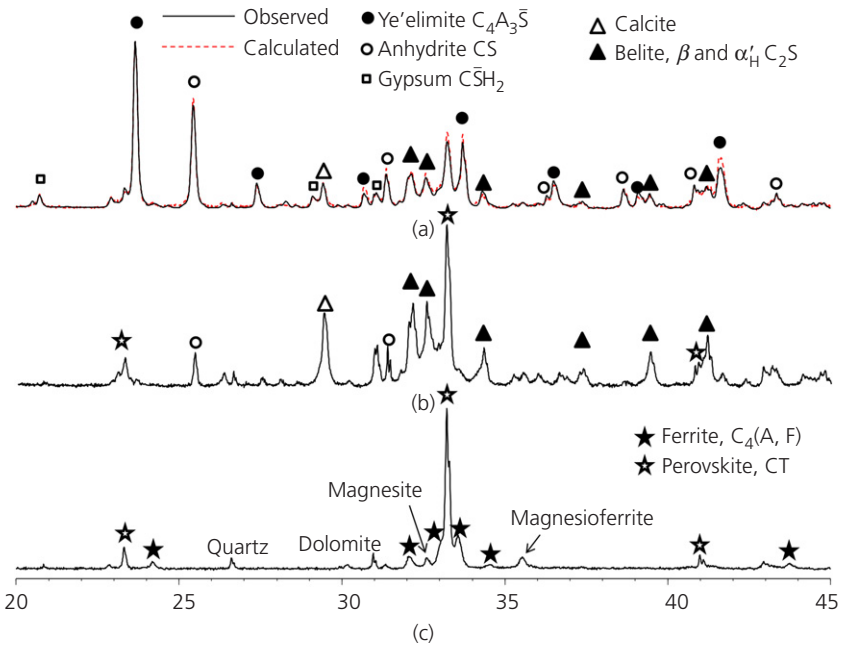

Figure 1. Diffraction patterns of (a) the CSA cement as received; (b) after potassium hydroxide (KOH)/sucrose extraction; and (c) after SAM and sodium carbonate extraction. The dashed curve in part (a) represents the Rietveld refinement

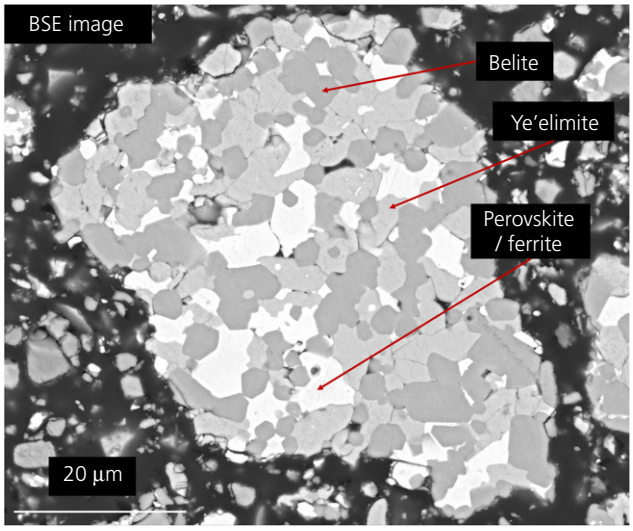

Figure 2. Back-scattering image of the CSA cement (BSE, back-scattered electron)

micrometres (Le Saoût *et al.*, 2019). These compositions were similar to those observed by Gloter *et al.* (2000) for the ferrite/perovskite phases in a calcium aluminate cement.

In order to confirm the amount of perovskites in the sample, a set of 266 images was processed by means of the Aphelion imaging software (Aphelion Dev, version 4.4.0). The whole process is composed of several steps, which use the following Aphelion groups of function: Gaussian filtering, segmentation in order to subtract from the surface the porosity filled by epoxy resin, morphological filter and segmentation to detect perovskite phases (Figure 3). According to the Delesse principle (Delesse, 1848), it can be assumed that the fractional area of a section plane taken up by perovskite phases is an estimate of the volume fraction. The mean value of the volume per cent of perovskites phases (ferrite and perovskite) deduced by image analysis has a value of 11 ± 2 vol%. This value can be compared to the sum of volume per cent of perovskite and ferrite deduced by XRD and equal to 12·7 vol% as Rietveld refinement permits both the weight and volume fraction to be obtained (Le Saoût *et al.*, 2011). Good agreement of the results can be observed, confirming the amount of perovskites in the cement.

Hydration of the CSA cement

Figure 4 shows the thermal power as a function of time for the CSA cement. The curves are similar to that observed in a calcium sulfate–ye'elimite system (Winnefeld and Barlag, 2010) except for the kinetic, which depends on many parameters such as the presence of alkalis or minor phases as $C_{12}A_7$ (Zajac *et al.*, 2019). The first peak observed with in situ experiments (Figure 4(b)) occurs when the water is added and can be assigned to wetting and early hydration process. After an induction period of about 2 h, two heat flow maxima occur at 3 and 5 h. Unlike in Portland cement where the addition of

Table 3. Atomic ratios for some phases in CSA calculated from energy dispersive spectroscopy

Phases/Formulae	Na	Ca	Mg	Fe	Al	Si	S	Ti	O
Ye'elimite	<1	402(5)	<1	28(4)	560(7)	7(2)	100(4)	<1	1600
$Ca_{4·02}$ $Al_{5·60}$ $Fe_{0·28}$ $Si_{0·07}$ $S_{1·01}$ O_{16}	402			595			100		
Belite	<1	192(6)	<1	1(1)	7(1)	89(6)	5(3)	<1	400
$Ca_{1·92}$ $Al_{0·07}$ $Si_{0·89}$ $S_{0·05}O_4$	192			102					
Ferrite	<1	198(1)	7(1)	133(1)	39(2)	10(1)	<1	8(1)	500
$Ca_{2·05}$ $Mg_{0·07}$ $Al_{0·39}$ $Fe_{1·33}$ $Si_{0·10}$ $Ti_{0·08}$ O_5	205			190					
Perovskite	<1	195(5)	5(1)	103(6)	29(4)	22(3)	<1	39(5)	518(7)
$Ca_{1·95}$ $Mg_{0·05}$ $Al_{0·29}$ $Ti_{0·39}$ $Fe_{1·03}$ $Si_{0·22}$ $O_{5·18}$	200			193					518

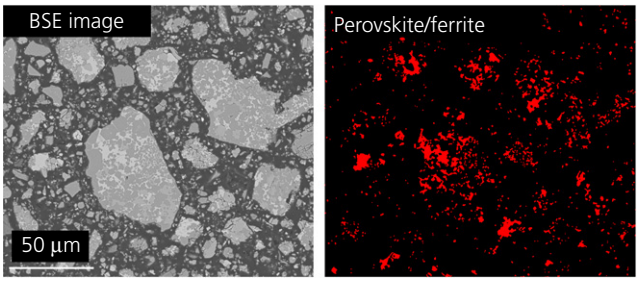

Figure 3. Back-scattering image of (a) the CSA cement and (b) the perovskite and ferrite phases after image analysis

10 mass% of zincite extends the induction period (no peak of hydration is observed in the calorimetric curve up to 80 h, experiment not shown), the addition of zincite shortened the induction period of about 10 min. A similar effect is observed when the finely ground quartz is added to the CSA cement, which indicates that the slight acceleration is due to the additional surface provided for the nucleation and growth of hydration products (Lothenbach *et al.*, 2008).

Figure 5 shows the amount of phases deduced from in situ XRD Rietveld analysis as a function of hydration time and measured heat flow. As previously observed, the solubility of calcium sulfates influences the initial period of hydration (Allevi *et al.*, 2016; Winnefeld and Barlag, 2009). The gypsum, which is more soluble than anhydrite, completely dissolves after 3 h, followed by the dissolution of anhydrite up to 8 h after the depletion of gypsum. In parallel, the dissolution of the ye'elimite phase occurs at the same time as the precipitation of the ettringite and AH_3 according to the reaction (Figure 6)

$$C_4A_3\bar{S} + 2C\bar{S}H_x + (38 - 2x)H \rightarrow C_6A\bar{S}_3H_{32} + 2AH_3$$

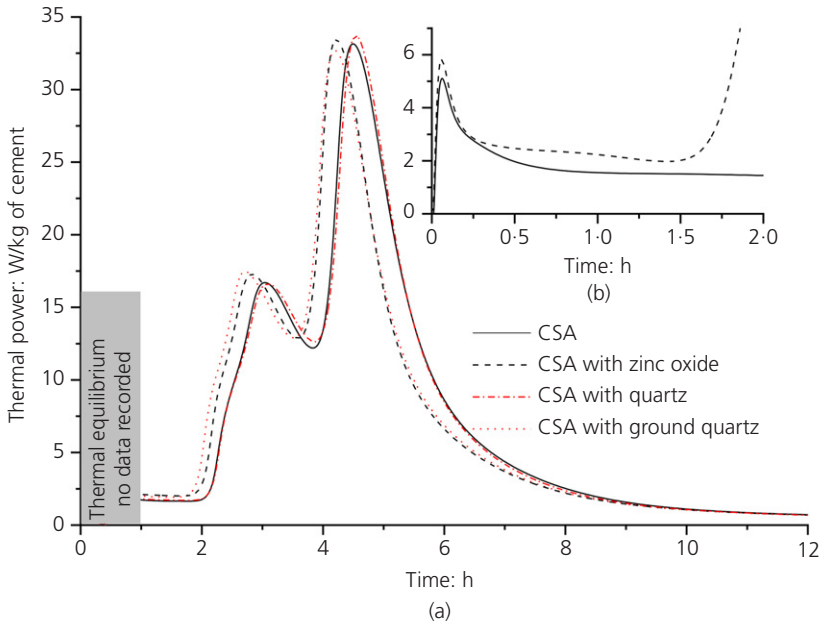

Figure 4. Heat flow development of mixtures with CSA cement and different fillers as a function of time: (a) between 0 and 12 h using external mixing; (b) (inset) between 0 and 2 h using internal mixing

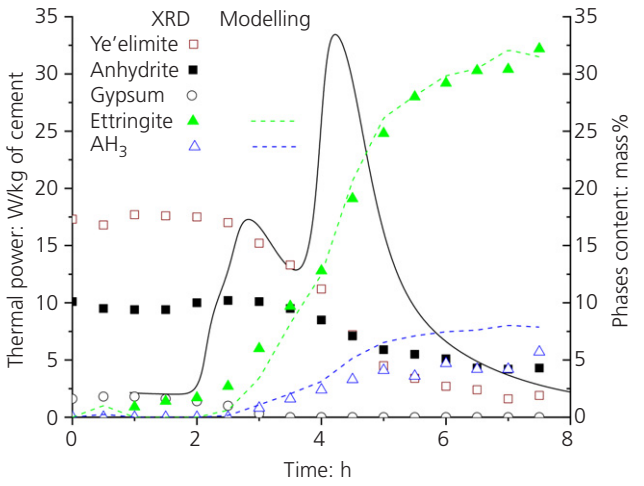

Figure 5. Phases content calculated from in situ XRD experiments (dotted points) and heat flow development (continuous lines) of CSA cement blended with zincite between 0 and 8 h. Dotted lines refer to the results of thermodynamic modelling

Some broad reflections of AH_3 were observed by XRD but, as previously reported (Le Saoût *et al.*, 2018), AH_3 is not well crystallised and is difficult to characterise using XRD, especially with an in situ analysis where the conditions lead to a lower signal-to-noise ratio. The precipitation of AH_3 with the ettringite is better highlighted by TGA experiments (Figure 7). The other phases are not represented as they do not show significant changes with hydration time up to 1 d. By combining experimental data based on the Rietveld XRD data for the ye'elimite and sulfate phases as a function of time with a thermodynamic equilibrium model, the nature and amount of hydrates formed as a function of time can be deduced. Thermodynamic modelling shows the formation of ettringite and AH_3 in microcrystalline form, in agreement with experimental data. The calculated amount of ettringite (dotted line in Figure 5) corresponds to the amount deduced by XRD and the difference for AH_3 can be explained by the X-ray amorphous part of the AH_3.

The retarding effect of zincite observed in the case of the hydration of OPC is not found for the CSA cement. For the CSA cement, alkali concentrations are much lower compared to OPC, resulting in a lower pH in the pore solution during the first hours of hydration (Le Saoût *et al.*, 2013; Winnefeld and Barlag, 2010). The pH values measured for the CSA and the OPC cements after 7 min of hydration (respectively, 10·4 and 13·2) are reported in Figure 8 with the solubility of zincite as a function of pH. The solubility (S) of zincite in mol/l is defined as the sum of the concentrations of soluble species Zn^{2+}, $Zn(OH)_2$, $Zn(OH)_3^-$ and $Zn(OH)_4^{2-}$. Based on the thermodynamic data provided by GEMS and Wang *et al.* (2001) (see Table 4), the mole distributions of the different species in equilibrium with zincite at various pH values are compared in Figure 8. The Gibbs energy formation is similar in both databases, except for zinc hydroxide, which explains the differences between the mole distributions and solubility. Unlike OPC where zincite dissolves and leads to the formation $Zn(OH)_4^{2-}$ that poisons nucleation and growth mechanisms, zincite is practically not soluble in the pore solution of the CSA cement at early age. Zincite can be considered practically inert in the CSA cement at early age and acts as a filler.

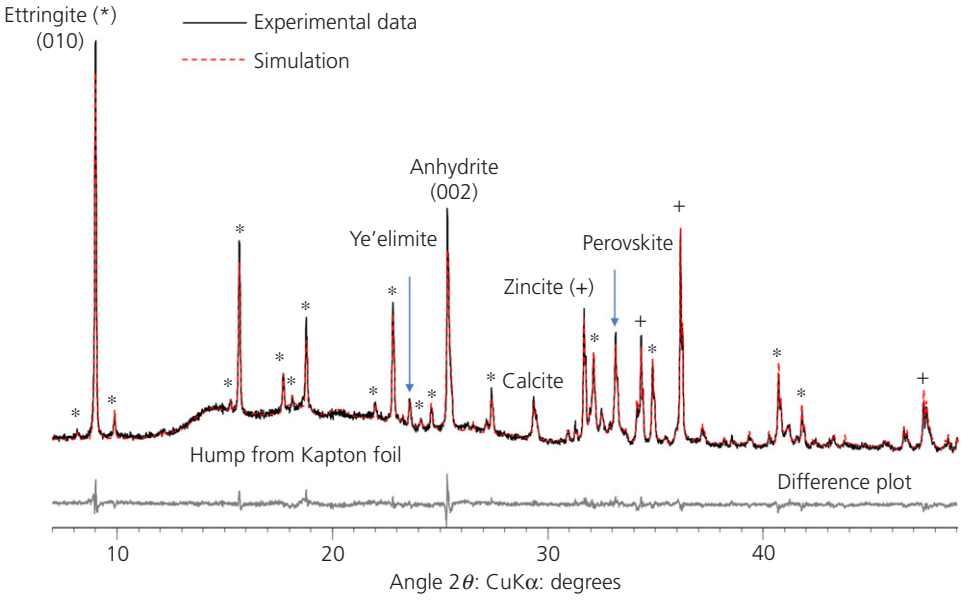

Figure 6. Refined pattern of the in situ XRD experiment of the CSA cement at 25°C and $w/c = 0{\cdot}7$ after 8 h of hydration

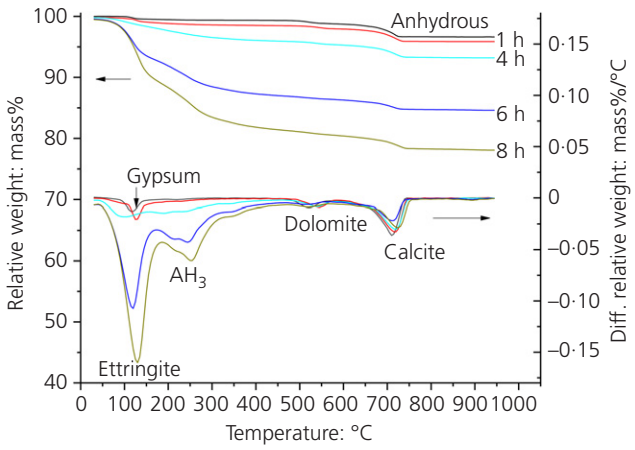

Figure 7. Weight loss recorded by TGA (top of the figure) and differential thermogravimetry data (bottom of the figure) of CSA cement between 0 and 8 h. A full-colour version of this figure can be found on the ICE Virtual Library (www.icevirtuallibrary.com)

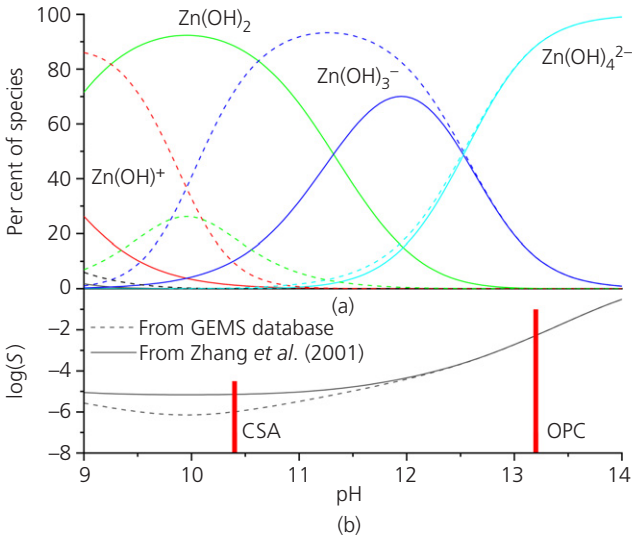

Figure 8. Zincite solubility (a) and soluble species (b) between pH 9 and 14 at T = 298·15 K according to the thermodynamic data reported in Zhang and Muhammed (2001) (dotted line) and in the GEMS database (solid line). Thick vertical lines indicate the pH of the pore solution after 7 min of hydration in CSA and OPC cements

Conclusion

The phase assemblage of a CSA cement has been investigated with a special focus on the perovskite phases. A modified selective extraction method highlighting the perovskite phases is presented to improve Rietveld refinement and facilitate EDX measurements. Perovskites are present in the cement in the form of brownmillerite and a phase with an average composition of $Ca_{1·95}Mg_{0·05}Al_{0·29}Ti_{0·39}Fe_{1·03}Si_{0·22}O_{5·18}$.

Table 4. The standard Gibbs energy of formation $\Delta_f G_0$ of some species in the system Zn(II)–H_2O at 298·15 K given by the GEMS database and the paper review (Wang *et al.*, 2001)

Species	$\Delta_f G_0$: kJ/mol	
	GEMS	Zhang and Muhammed (2001)
H_2O	−237·18	−237·14 ± 0·04
OH^-	−157·27	−157·22 ± 0·07
Zn^{2+}	−147·3	−147·2 ± 0·4
Zincite	−320·5	−320·5 ± 0·4
$Zn(OH)^+$	−339·7	−342 ± 3
$Zn(OH)_2^0$	−519·3	−528 ± 2
$Zn(OH)_3^-$	−700	−698 ± 2
$Zn(OH)_4^{2-}$	−865	−860 ± 3

The hydration of the CSA cement has been followed at early age where the ye'elimite reacts with calcium sulfate to produce ettringite and AH_3. The zincite behaves as a filler in the CSA cement and does not present a strong retardant effect as in OPC, which may result in greater potential use.

Acknowledgements

The authors would like to acknowledge Alain Diaz for sample preparation for the SEM experiments and Vicat for supplying the cement.

REFERENCES

Allevi S, Marchi M, Scotti F, Bertini S and Cosentino C (2016) Hydration of calcium sulphoaluminate clinker with additions of different calcium sulphate sources. *Materials and Structures* **49(1–2)**: 453–466.

Álvarez-Pinazo G, Cuesta A, García-Maté M *et al.* (2012) Rietveld quantitative phase analysis of yeelimite-containing cements. *Cement and Concrete Research* **42(7)**: 960–971.

Aranda MAG and De la Torre AG (2013) Sulfoaluminate cement. In *Eco-Efficient Concrete* (Pacheco-Torgal F, Jalali S, Labrincha J and John VM (eds)). Woodhead Publishing, Cambridge, UK, pp. 488–522.

Arliguie G and Grandet J (1985) Etude par calorimétrie de l'hydratation du ciment Portland en présence de zinc. *Cement and Concrete Research* **15(5)**: 825–832 (in French).

Ataie FF, Juenger MCG, Taylor-Lange SC and Riding KA (2015) Comparison of the retarding mechanisms of zinc oxide and sucrose on cement hydration and interactions with supplementary cementitious materials. *Cement and Concrete Research* **72**: 128–136.

Barth TFW and Posnjak E (1932) Spinel structures: with and without variate atom equipoints. *Zeitschrift Für Kristallographie – Crystalline Materials* **82**: 325–341.

Belaïd F, Arliguie G and François R (2001) Porous structure of the ITZ around galvanized and ordinary steel reinforcements. *Cement and Concrete Research* **31(11)**: 1561–1566.

Bolio-Arceo H and Glasser FP (1998) Zinc oxide in cement clinkering: part 1. Systems CaO–ZnO–Al_2O_3 and CaO–ZnO–Fe_2O_3. *Advances in Cement Research* **10(1)**: 25–32, https://doi.org/10.1680/adcr.1998.10.1.25.

Calos NJ, Kennard CH, Whittaker AK and Davis RL (1995) Structure of calcium aluminate sulfate $Ca_4Al_6O_{16}S$. *Journal of Solid State Chemistry* **119(1)**: 1–7.

De la Torre ÁG, López-Olmo MG, Álvarez-Rua C, García-Granda S and Aranda MAG (2004) Structure and microstructure of gypsum and its relevance to Rietveld quantitative phase analyses. *Powder Diffraction* **19(3)**: 240–246.

Delesse A (1848) Procédé mécanique pour déterminer la composition des roches. *Annales des Mines* **13(4)**: 379–388 (in French).

De Rincón OT, Pérez O, Paredes E *et al.* (2002) Long-term performance of ZnO as a rebar corrosion inhibitor. *Cement and Concrete Composites* **24(1)**: 79–87.

Effenberger H, Kirfel A and Will G (1983) Untersuchungen zur Elektronendichteverteilung im Dolomit CaMg $(CO_3)_2$. *Tschermaks Mineralogische Und Petrographische Mitteilungen* **31(1–2)**: 151–164 (in German).

Établissements Poliet & Chausson (1935) *Nouveau ciment et son procédé de fabrication*. French Patent FR 780.747, May (in French).

Fernández Olmo I, Chacon E and Irabien A (2001) Influence of lead, zinc, iron (III) and chromium (III) oxides on the setting time and strength development of Portland cement. *Cement and Concrete Research* **31(8)**: 1213–1219.

García-Maté M, Santacruz I, Cuesta A *et al.* (2015) Amorphous determination in calcium sulfoaluminate materials by external and internal methods. *Advances in Cement Research* **27(7)**: 417–423, https://doi.org/10.1680/adcr.14.00026.

Garg N and White CE (2017) Mechanism of zinc oxide retardation in alkali-activated materials: an in situ X-ray pair distribution function investigation. *Journal of Materials Chemistry A* **5(23)**: 11794–11804.

Gartner E (2004) Industrially interesting approaches to 'low-CO_2' cements. *Cement and Concrete Research* **34(9)**: 1489–1498.

Gloter A, Ingrin J, Bouchet D, Scrivener K and Colliex C (2000) TEM evidence of perovskite–brownmillerite coexistence in the Ca $(Al_xFe_{1-x})O_{2.5}$ system with minor amounts of titanium and silicon. *Physics and Chemistry of Minerals* **27(7)**: 504–513.

Goetz-Neunhoeffer F and Neubauer J (2006) Refined ettringite $(Ca_6Al_2(SO_4)_3(OH)_{12}\ 26H_2O)$ structure for quantitative X-ray diffraction analysis. *Powder Diffraction* **21(1)**: 4–11.

Göttlicher S and Vegas A (1988) Electron-density distribution in magnesite ($MgCO_3$). *Acta Crystallographica Section B: Structural Science, Crystal Engineering and Materials* **44(4)**: 362–367.

Gualtieri AF (2000) Accuracy of XRPD QPA using the combined Rietveld-RIR method. *Journal of Applied Crystallography* **33(2)**: 267–278.

Hjorth L and Lauren KG (1971) Belite in Portland cement. *Cement and Concrete Research* **1(1)**: 27–40.

Hummel W, Berner U, Curti E, Pearson FJ and Thoenen T (2002) Nagra/PSI chemical thermodynamic data base 01/01. *Radiochimica Acta* **90(9–11)**: 805–813.

Jansen D, Goetz-Neunhoeffer F, Stabler C and Neubauer J (2011) A remastered external standard method applied to the quantification of early OPC hydration. *Cement and Concrete Research* **41(6)**: 602–608.

Kirfel A and Will AG (1990) Charge density in anhydrite, $CaSO_4$, from X-ray and neutron diffraction measurements. *Acta Crystallographica Section B* **36(12)**: 2881–2890.

Klein A and Troxell GE (1958) Studies of a calcium sulfoaluminate admixtures for expansive cements. *ASTM Proceedings* **58**: 986–1008.

Kulik DA, Wagner T, Dmytrieva SV *et al.* (2013) GEM-Selektor geochemical modeling package: revised algorithm and GEMS3K numerical kernel for coupled simulation codes. *Computational Geosciences* **17(1)**: 1–24.

Lejbina LP (1969) Quantitative analysis of tricalcium aluminate and tetracalcium aluminoferrite in the same sample. *Ogneupory SSSR* **34**: 52–56.

Le Saoût G, Kocaba V and Scrivener K (2011) Application of the Rietveld method to the analysis of anhydrous cement. *Cement and Concrete Research* **41(2)**: 133–148.

Le Saoût G, Lothenbach B, Hori A, Higuchi T and Winnefeld F (2013) Hydration of Portland cement with additions of calcium sulfoaluminates. *Cement and Concrete Research* **43**: 81–94.

Le Saoût G, Lothenbach B, Taquet P, Fryda H and Winnefeld F (2018) Hydration of calcium aluminate cement blended with anhydrite. *Advances in Cement Research* **30(1)**: 24–36, https://doi.org/10.1680/jadcr.17.00045.

Le Saoût G, Idir R and Roux JC (2019) Characterization of perovskites in a calcium sulfo aluminate cement. In *14th International Congress for Applied Mineralogy (ICAM 2019)* (Galgolev S (ed.)). Springer Nature Switzerland, Cham, Switzerland.

Lothenbach B, Le Saoût G, Gallucci E and Scrivener K (2008) Influence of limestone on the hydration of Portland cements. *Cement and Concrete Research* **38(6)**: 848–860.

Lothenbach B, Kulik DA, Matschei T *et al.* (2019) Cemdata18: a chemical thermodynamic database for hydrated Portland cements and alkali-activated materials. *Cement and Concrete Research* **115**: 472–506.

Moore PB and Araki T (1972) Atomic arrangement of merwinite, $Ca_3Mg[SiO_4]_2$, an unusal dense-packed structure of geophysical interest. *American Mineralogist* **57(9–10)**: 1355–1374.

Mumme WG, Hill RJ, Bushnell-Wye G and Segnit ER (1995) Rietveld crystal structure refinements, crystal chemistry and calculated powder diffraction data for the polymorphs of dicalcium silicate and related phases. *Neues Jahrbuch Für Mineralogie Abhandlungen* **169(1)**: 35–68.

Odler I (2000) *Special Inorganic Cements: Modern Concrete Technology 8*. E & FN Spon, London, UK.

Redhammer GJ, Tippelt G, Roth G and Amthauer G (2004) Structural variations in the brownmillerite series $Ca_2(Fe, Al)O_5$: single-crystal X-ray diffraction at 25°C and high temperature X-ray powder diffraction (25°C < T < 1000°C). *American Mineralogist* **89(2–3)**: 405–420.

Saalfeld H and Depmeier W (1972) Silicon-free compounds with sodalite structure. *Crystal Research and Technology* **7(1–3)**: 229–233.

Saafeld H and Wedde M (1974) Strukturen des Hydrargillits und der Zwischenstufen beim Entwaessern. *Zeitschrift für Kristallographie* **139S(1–2)**: 129–135 (in German).

Sasaki S (1997) Radial distribution of electron density in magnetite, Fe_3O_4. *Acta Crystallographica Section B: Structural Science* **53(5)**: 762–766.

Sasaki S, Prewitt CT and Bass JD (1987) Orthorhombic perovskite $CaTiO_3$ and $CdTiO_3$: structure and space group. *Acta Crystallographica Section C: Structural Chemistry* **43(9)**: 1668–1674.

Senff L, Tobaldi DM, Lemes-Rachadel P, Labrincha JA and Hotza D (2014) The influence of TiO_2 and ZnO powder mixtures on photocatalytic activity and rheological behaviour of cement pastes. *Construction and Building Materials* **65**: 191–200.

Taylor D (1984) Thermal expansion data. I. Binary oxides with the sodium chloride and wurtzite structure, MO. *Transactions and Journal of the British Ceramic Society* **83**: 5–9.

Taylor HFW (1997) *Cement Chemistry*. Thomas Telford, London, UK.

Toyama K and Terakado Y (2015) Differential dissolution technique for the geochemical separation of the calcite and dolomite of dolomitic limestones. *Geochemical Journal* **49(5)**: 567–570.

Wadsö L (2005) Applications of an eight-channel isothermal conduction calorimeter for cement hydration studies. *Cement International* **5(5)**: 94–101.

Wang J (2010) *Hydration Mechanism of Cements Based on Low-CO_2 Clinkers Containing Belite, Ye'elimite and Calcium Alumino-Ferrite*. PhD dissertation, University of Lille, Lille, France.

Wang Y and Su M (1994) The third cement series in China. *World Cement* (August): 6–10.

Wartchow R (1989) Datensammlung nach der 'learnt profile'-Methode (LP) für Calcit und Vergleich mit der 'background peak background'.-Methode (BPB). *Zeitschrift für Kristallographie* 300–303 (in German).

Winnefeld F and Barlag S (2009) Influence of calcium sulfate and calcium hydroxide on the hydration of calcium sulfoaluminate clinker. *ZKG International* **12**: 42–53.

Winnefeld F and Barlag S (2010) Calorimetric and thermogravimetric study on the influence of calcium sulfate on the hydration of ye'elimite. *Journal of Thermal Analysis and Calorimetry* **101(3)**: 949–957.

Winnefeld F and Lothenbach B (2010) Hydration of calcium sulfoaluminate cements – experimental findings and thermodynamic modeling. *Cement and Concrete Research* **40(8)**: 1239–1247.

Zajac M, Skocek J, Bullerjahn F *et al.* (2019) Early hydration of ye'elimite: insights from thermodynamic modelling. *Cement and Concrete Research* **120**: 152–163.

Wang M, Zhang Y and Muhammed M (2001) Critical evaluation of thermodynamics of complex formation of metal ions in aqueous solutions VI. Hydrolysis and hydroxo-complexes of Zn^{2+} at 298.15 K. *Hydrometallurgy* **60(3)**: 215–236.

Zhang L, Su M and Wang Y (1999) Development of the use of sulfo- and ferroaluminate cements in China. *Advances in Cement Research* **11(1)**: 15–21, https://doi.org/10.1680/adcr.1999.11.1.15.